CBP Tech Note-233
LCC-0066

A New Structure for the NLC Positron Pre-Damping Ring Lattice

Andrzej Wolski
Lawrence Berkeley National Laboratory

June 21st, 2001

Abstract

The NLC positron source is specified to produce a beam of normalized edge emittance 30,000 mm-mrad. It is not practicable, using a single damping ring, to damp this emittance to meet the specification for injection into the main linac, so a pre-damping ring is used to reduce the emittance to a value at least as small as that of the electron beam from the source. In this note, we describe the design of a pre-damping ring based on a double-bend achromat structure, as opposed to the previously investigated theoretical minimum emittance cell. The lattice meets the specifications for damping and has close to the required acceptance, and has advantages over previous lattices, in terms of component specifications and design flexibility.

1 Introduction

The injector complex for the NLC uses identical main damping rings for each beam, that are specified to reduce the normalized emittance from 150 mm-mrad horizontally and vertically, to below 3 mm-mrad horizontally and 0.02 mm-mrad vertically. With a repetition rate of 120 Hz, this damping can be achieved using a single ring for each beam. Recent design work leading to a suitable lattice for the main damping rings is described in reference 1. To achieve the very low emittance and required damping rate, the lattice uses strong focusing magnets, and a high field (2.15 T) wiggler with a length of approximately 46 m. The narrow aperture of these magnets limits the acceptance of the ring. The positron source is specified to produce a beam with edge emittance 30,000 mm-mrad. It is not practicable to damp such a large emittance to the values required for injection into the main linac in a single ring. Furthermore, the main damping rings will not have the transverse acceptance required for a beam with such a large emittance.

The positron source parameters and the main damping ring specifications lead to the need for a pre-damping ring, that will reduce the emittance from 30,000 mm-mrad, to below 150 mm-mrad for injection into the main damping ring. One significant difference between the pre-damping ring and the main damping rings is that the emittance specification on the pre-damping ring is much more relaxed. Rapid damping is still required, but an equilibrium emittance of around 100 mm-mrad or less will be sufficient. Also, it is not necessary to produce a flat beam, so the alignment tolerances and coupling correction will be much looser than in the main rings. However, the pre-damping ring will require a relatively large acceptance, which will impact the design of the lattice and its magnetic elements.

Previous work on the pre-damping ring lattice has based the design on a racetrack structure[2,3]. The ZDR design, for example, used 15 FOBO cells in each arc, to achieve an equilibrium emittance of 77 mm-mrad. The densely packed lattice had a circumference of 171 m. All the damping was provided by the main arc dipoles, which needed a field of 1.8 T to meet the damping specification. We have recently considered a design using TME cells instead of FOBO cells in the arcs, and which is therefore similar to the main damping rings. Although the number of cells required to reach the emittance is significantly reduced compared to the FOBO lattice, we have found that the TME lattice presents particular problems:

- Optimizing the dynamic aperture to achieve the specified acceptance is difficult, since the lattice has low symmetry, and the available nonlinear elements are used to correct the chromaticity.
- Improving the dynamic aperture requires significant detuning of the cell from the TME condition, to raise the dispersion at the chromatic sextupoles and reduce the natural chromaticity, thus reducing the strengths of the sextupoles.
- The large dispersion leads to a large momentum compaction, and hence a large RF voltage is needed to provide sufficient momentum acceptance. Our most recent lattice required a voltage of 3.4 MV, and seven RF cavities.
- Packing a number of systems into a single straight (including injection, RF, damping wiggler, and circumference correction chicane) severely affects the tuning flexibility, and makes it difficult to limit the beta functions to the low values needed to improve the acceptance. Adjustment of the circumference correction chicanes, for example, becomes problematic.
- Limited available space for the damping wiggler leads to a high peak field requirement, of the order 1.2 T. This is difficult to achieve while maintaining a large aperture.

The design presented in this note avoids the above problems associated with the TME lattice, by adopting a 10-fold symmetric double-bend achromat (DBA) structure. The DBA lattice is able to reach sufficiently low emittance with fewer components compared to the FOBO lattice. It provides space for harmonic sextupoles to allow optimization of the dynamic aperture, so the dispersion, and hence the momentum compaction and the RF voltage can be kept to low values compared with the TME lattice. Furthermore, the structure allows separation of the different components, so that the damping wiggler, injection/extraction systems, RF cavities and chicane are all placed in separate straights; this greatly assists lattice design, since the different cells can be optimized independently, and should also ease engineering constraints, for example in locating photon stops to absorb the synchrotron radiation from the dipoles and wiggler.

2 Lattice Parameters and Structure

Parameters driving the design of the pre-damping ring are shown in Table 1; these are essentially the repetition frequency, and the injected and extracted emittances. The minimum machine circumference is fixed from the number of bunch trains stored, the number of bunches per train and the inter-bunch spacing, and the kicker rise/fall time. Lattice parameters are given in Table 2, and wiggler parameters in Table 3.

Table 1: "External" parameters.

Bunches per train	N_b	190
bunch-to-bunch spacing[a]	τ_b /ns	1.4
kicker rise/fall time	τ_k /ns	100
collider repetition rate	f /Hz	120
injected horizontal/vertical emittance (edge [a])	$\gamma\varepsilon_{inj}$ /mm mrad	30,000
extracted horizontal emittance (rms)	$\gamma\varepsilon_{x,ext}$ /mm mrad	<150
extracted vertical emittance (rms)	$\gamma\varepsilon_{y,ext}$ /mm mrad	<150

[a] For a discussion of the edge emittance, see Section 6.

Table 2: Principal lattice parameters.

Energy	E /GeV	1.98
Number of bunch trains stored	N_{train}	2
Store time (horizontal, vertical) [b]	N_τ	3.00, 3.03
Circumference	C /m	230.933
Basic cell type		DBA
Basic cell length	/m	23.0933
Number of cells		10
Dipole field	B_0 /T	1.383
Tunes (horizontal, vertical, synchrotron)	Q_x, Q_y, Q_s	11.465, 5.388, 0.0114
Natural chromaticity (horizontal, vertical)	ξ_x, ξ_y	-24.771, -13.391
Normalized natural emittance	$\gamma\varepsilon_0$ /mm mrad	59.7
Damping times	$\tau_x, \tau_y, \tau_\varepsilon$ /ms	5.85, 5.81, 2.89
Assumed coupling	κ	5 %
Assumed injected emittance (rms)	$\gamma\varepsilon_{inj}$ /mm mrad	21,000
Extracted emittance (horizontal, vertical) (rms)	$\gamma\varepsilon_{ext}$ /mm mrad	127.3, 70.25
Ratio of vertical equilibrium to extracted emittance	$\varepsilon_{y0} / \varepsilon_{y,ext}$	0.042
Momentum compaction	α	2.00×10^{-3}
RF voltage	V_{rf} /MV	1.516
RF acceptance	ε_{rf}	1.5 %
RF frequency	f_{rf} /MHz	714
Harmonic number	h	550
Equilibrium energy spread (rms)	σ_δ	0.0777 %
Equilibrium bunch length (rms)	σ_z /mm	5.14

[b] The store time is the number of damping times for which each train is stored.

Table 3: Wiggler parameters

Wiggler peak field	$\hat{B}_w$ /T	1.4
Wiggler period	λ_w /m	1.0
Wiggler total length	L_w /m	49.5
Integrated wiggler field	$\int \hat{B}_w^2 ds$ /T^{2}m	48.51
Energy loss/turn, dipoles + wiggler	$U_0 + U_w$ /keV	284 + 241 = 525
Energy loss ratio	F_w	0.849

Note that we calculate the extracted emittance from an "effective rms" value for the injected beam emittance. We assume that the effective rms emittance is given by $\gamma\varepsilon_{rms} \approx 0.7\gamma\varepsilon_{edge}$ (see Section 6, equation (2)).

The basic double-bend achromat structure of a single cell is shown in Figure 1. The dispersion is close to zero outside of the achromat; the wiggler generates the small residual dispersion. The achromat uses two quadrupole doublets, and three chromatic sextupoles. The harmonic sextupoles are located outside of the achromat. Use is made of the significant vertical focusing from the wiggler, to reduce the number of quadrupoles in the straight section: only three are required in the wiggler section. The beta functions are moderate, below 18 m horizontally and vertically throughout the cell.

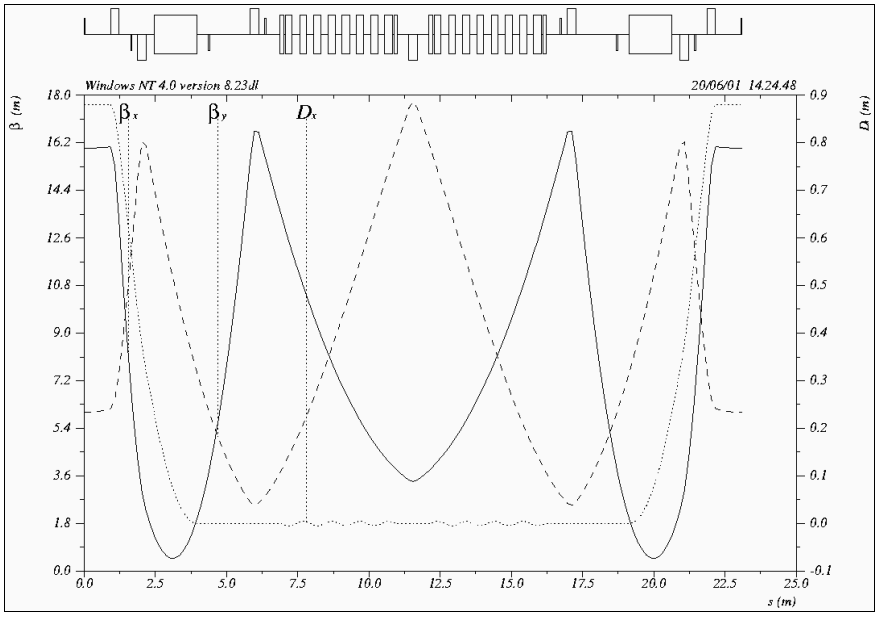

Figure 1

Lattice functions in one wiggler cell.

Other types of cell are constructed for the RF cavities (Figure 2), chicane (Figure 3), and injection and extraction systems (Figure 4). Note that the structure and lattice functions in these different types of cell are very similar. The main difference when compared to the wiggler cell, is the use of a quadrupole doublet outside the achromat. The beta

functions are very slightly larger, but still below 20 m. The geometry of the lattice is simplified by having the cells the same length, and the spacing of the dipoles the same in each case; thus, the layout is a regular decagon.

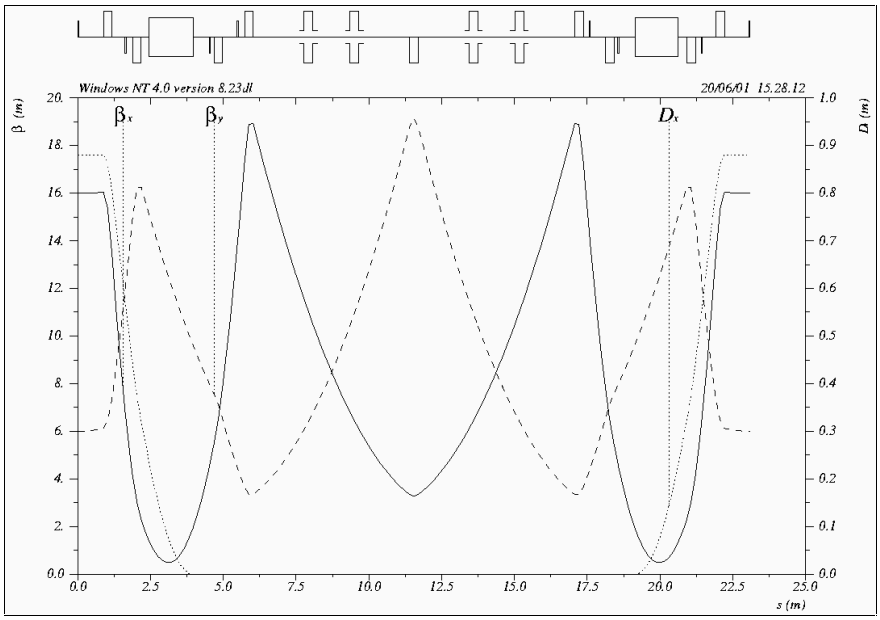

Figure 2

Lattice functions in the RF cell.

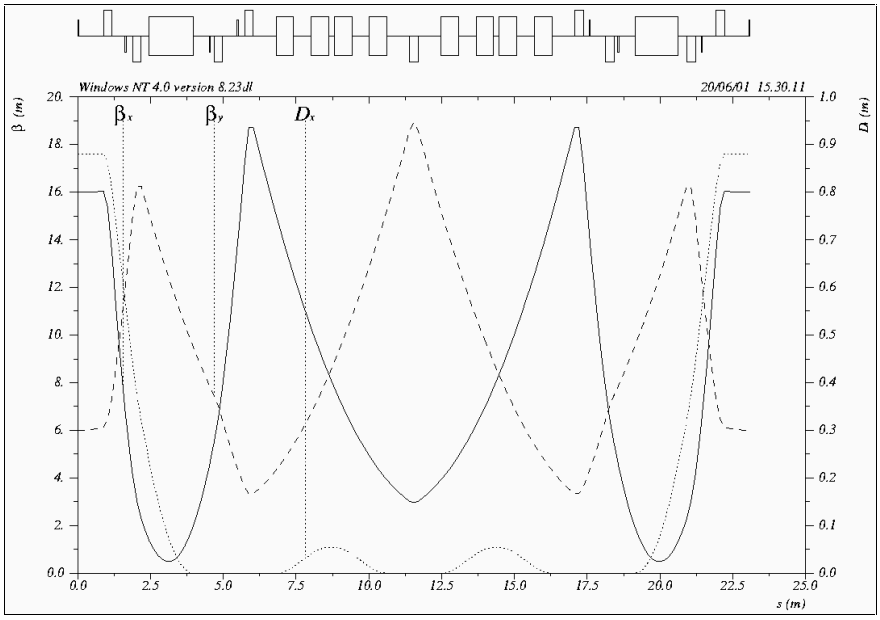

Figure 3

Lattice functions in the chicane cell.

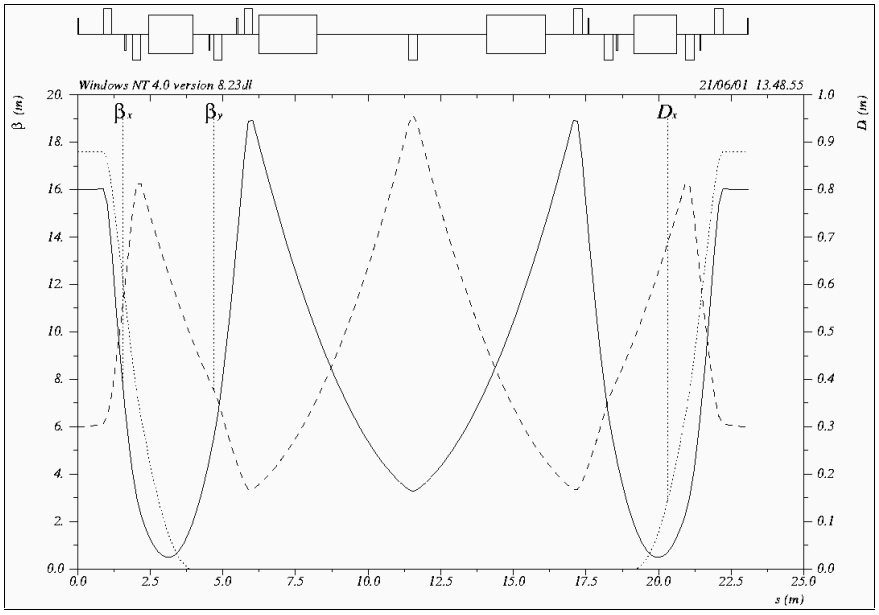

Figure 4

Lattice functions in the extraction cell.

2.1 RF Cell

There is more than sufficient space for four RF cavities. The RF system requires that the distance between the centerlines of the cavities is a whole number plus three-quarters of an RF wavelength; adjacent cavities are separated by 3¾ wavelengths, and cavities on either side of the central quadrupole are separated by 9¾ wavelengths. It is assumed at present that the cavities will be the same design as used in the main damping rings[4], being HOM-damped structures based on the PEP-II design. Studies of instabilities driven by modes in the cavities have yet to be carried out for the pre-damping ring, though we note that in the case of the main damping rings, only a few modes transverse and longitudinally are above the damping threshold[5], and growth rates for these modes can readily be dealt with by feedback systems.

2.2 Chicanes

The present design uses two separate chicanes, each being identical in design to that used in the main damping ring, and allowing adjustment of the circumference over ±2 mm. Thus, the total circumference adjustment range is ±4 mm. The use of the same system in the pre-damping ring as in the main damping ring in itself brings some benefits. The larger momentum compaction in the pre-damping ring (by a factor of seven) implies greater sensitivity to circumference changes through environmental effects, although with a smaller circumference, these effects should themselves be smaller. Thus, greater circumference variability is desirable in the pre-damping ring. Using two chicanes rather than one eases the technical requirements and minimizes the retuning required in the circumference adjustment; it also allows the symmetry of the cell to be maintained.

2.3 Injection/Extraction systems

We have assumed the same design for the injection/extraction kickers and septa as given in the NLC ZDR[6]; the kickers and septa are each 2 m long, the kickers providing a deflection of 8 mrad (injection) and 6.6 mrad (extraction), and the septa a deflection of 150 mrad. The central defocusing quadrupole provides additional bending for the

injected/extracted beam. The circumference of the lattice allows for a kicker rise/fall time of 119 ns. The geometry in the injection region is shown in Figure 5. With the present design, the kicked beam is 77.8 mm off-axis relative to the stored beam at the entrance to the septum. At the location of the next quadrupole following the last septum in the direction of the extracted beam, the kicked beam is 423 mm off-axis, with respect to the stored beam. The technical constraints so far look reasonable; the symmetry of the lattice, with injection and extraction on opposite sides of the ring, allow flexibility in increasing the length of these systems if necessary, at the cost of increasing the overall circumference.

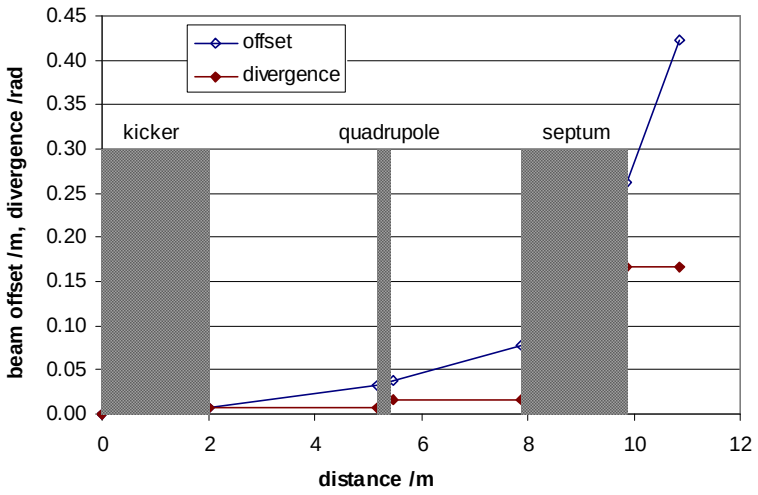

Figure 5

Injection geometry (beam travels from the right).

2.4 Overall Structure

The overall structure of the pre-damping ring lattice is shown in Figure 6. The sequence of cells can be chosen for practical convenience: there are no fundamental lattice issues. Thus, the RF cell may be located anywhere from the injection to the extraction straight (following the direction of the beam), where the cavities will not be subject to any transient beam loading resulting from in injection/extraction cycle. Although the injection and extraction cells are shown diametrically opposite, to correspond more closely to the current overall configuration of the injector systems[7], this in itself is not a lattice requirement, and relative repositioning of these straights presents no lattice problems.

3 Dynamics and Acceptance

3.1 Chromatic Properties

The achromat is designed to provide (between the dipoles) large horizontal dispersion and good separation of the horizontal and vertical beta functions, to allow correction of the chromaticity with moderate sextupole strengths. Constraining the beta functions to low values throughout the lattice helps keep the natural chromaticity of the lattice low. Harmonic sextupoles, placed in regions of zero dispersion, can be used to correct higher order chromaticity, as well as nonlinear betatron parameters.

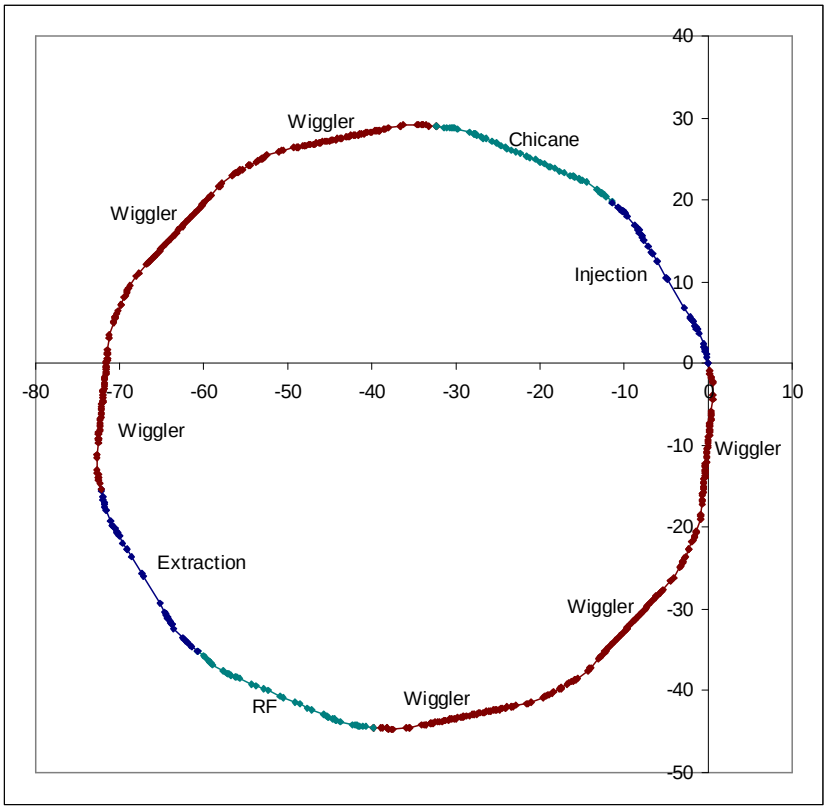

Figure 6

Overall structure of the pre-damping ring. The scales are in metres. The beam circulates clockwise.

Figure 7 shows the variation in tune with momentum up to ±2 % momentum deviation. We note that adjusting for slightly positive horizontal chromaticity can reduce the total variation in horizontal tune. The tune variation looks sufficiently small to allow reasonable dynamic momentum acceptance. We have not yet carried out an analysis of the harmonic sextupoles tuning, and further optimization may be possible.

The working point in tune space is shown in Figure 8. We are not concerned about the proximity to coupling resonances: low betatron coupling is not a performance requirement for the pre-damping ring, since the specification on extracted emittances places equal upper limits in the two transverse planes.

3.2 Dynamic Aperture

To assist with injection efficiency, the dynamic aperture of the lattice is improved through the use of harmonic sextupoles. The present specification of the lattice is for a transverse acceptance corresponding to an edge emittance of 45,000 mm-mrad (see Section 6); this is derived from the nominal injected beam edge emittance of 30,000 mm-mrad, plus 50% to allow for mismatches and jitter. We note that a particle at the dynamic acceptance limit has a maximum offset from the design orbit given by:

$$\hat{x} = \sqrt{2\beta\varepsilon_{edge}} + \eta\delta \qquad (1)$$

where η is the dispersion, and δ is the momentum deviation.

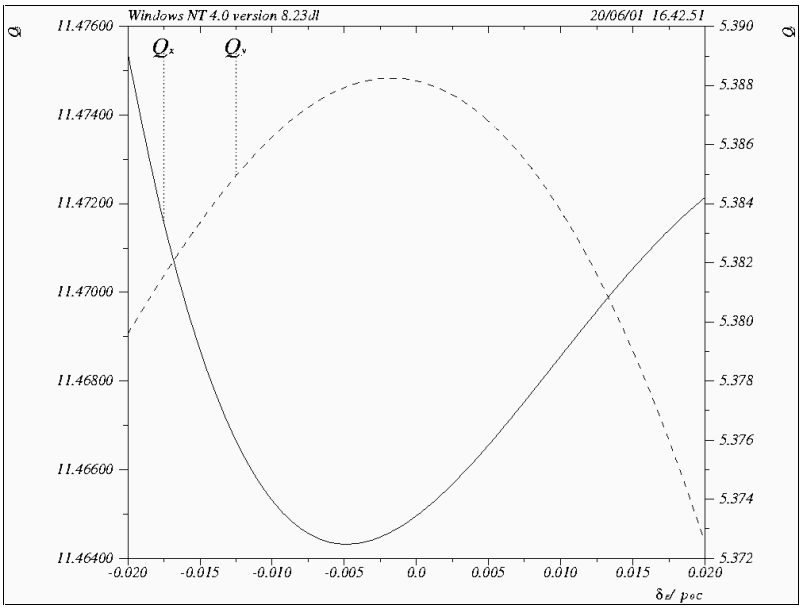

Figure 7

Tune shift with momentum up to ±2 % momentum deviation.

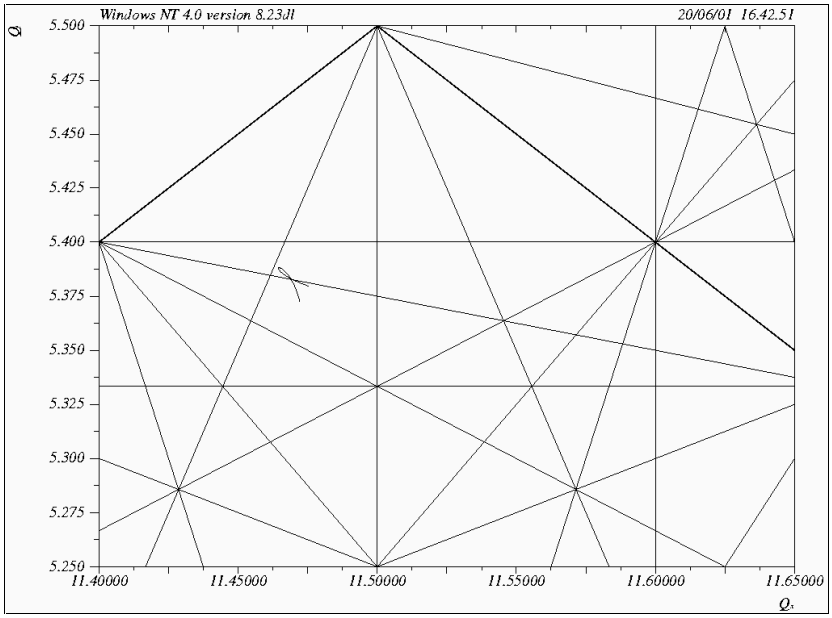

Figure 8

Working point in tune space. The nominal working point is (11.465,5.388): the curved line shows variation in tunes up to ± 2% momentum deviation. Resonance lines up to fifth order are shown.

The specified energy acceptance is ±1.5%. This again includes a margin of 50% over the nominal beam properties (1% half-width energy spread) to allow for jitter. The equilibrium bunch length is 5.14 mm with an energy spread of 0.0777% (see Table 1): thus, we expect that soon after injection, the bunch length is likely to filament to around 66 mm. With an RF wavelength of 420 mm, and rapid longitudinal damping, this is not anticipated to be a problem.

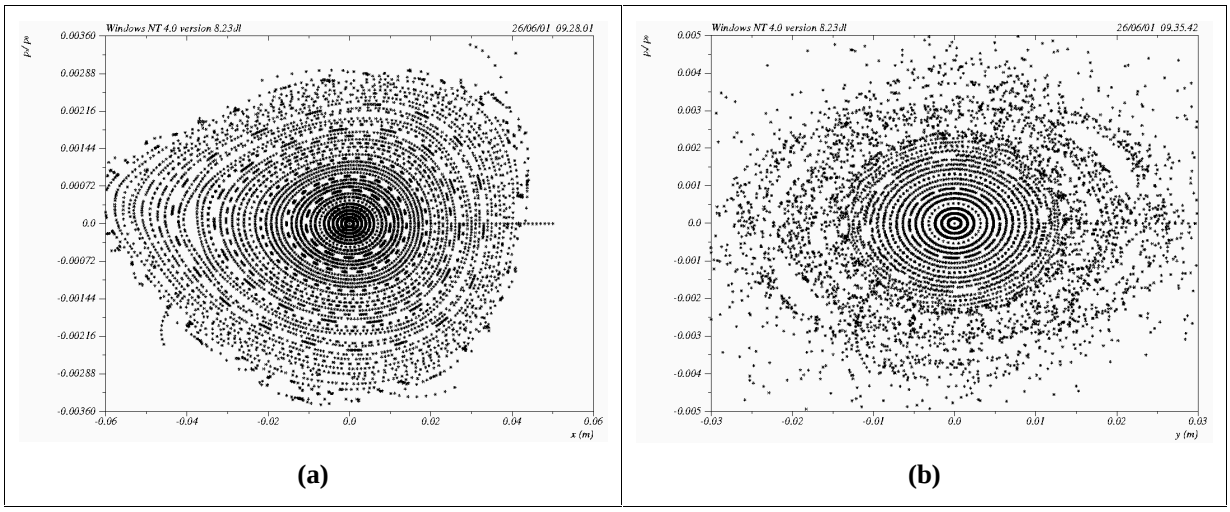

(a) **(b)**

Figure 9

(a) Horizontal and (b) vertical phase space portraits for on-momentum particles.

Horizontal and vertical phase space portraits for on-momentum particles are shown in Figure 9. In the horizontal plane, the dynamics show small nonlinearities for amplitudes approaching 0.04 m.

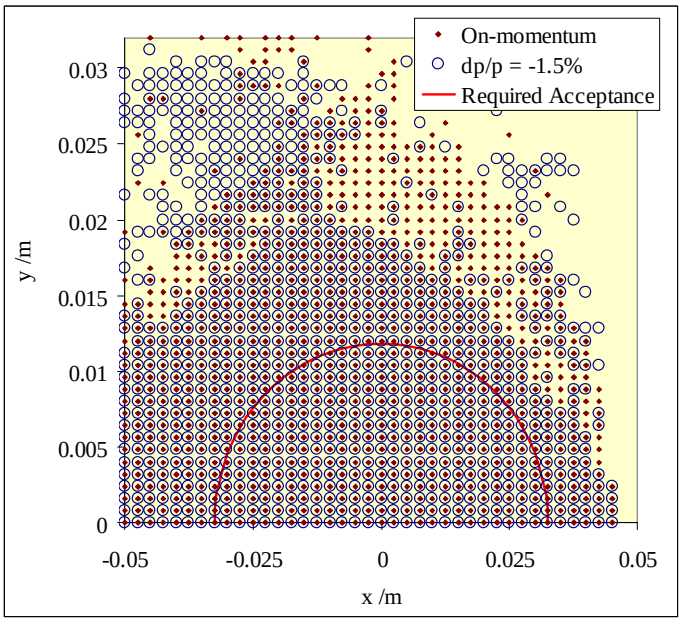

Figure 10

Dynamic apertures for particles with zero and –1.5% momentum deviation.

The dynamic apertures, for particles with zero and –1.5% momentum deviation, are shown in Figure 10. The dynamic aperture is calculated by tracking 200 turns, with the observation point at the center of an achromat, i.e. at the midpoint of the sextupole correcting the horizontal chromaticity. At this location, the horizontal beta function has a value of 16.0 m, the vertical beta function is 6.0 m, and the horizontal dispersion is 0.881 m. The required acceptance also shown in Figure 10 is calculated using these values in (1), with the edge acceptance 45,000 mm-mrad, and energy acceptance 1.5% half-width. The dynamic aperture appears to be beyond the required limit. We have not so far included multipole field errors in the magnets, although we do not expect this to affect the dynamic aperture to such an extent that the specified acceptance cannot be achieved. We have so far carried out only a preliminary optimization of the dynamic aperture. It is to be expected that with more work, optimizing the design of the individual cells, and the locations and strengths of the harmonic sextupoles, the dynamic aperture may be improved.

3.3 Acceptance

As we have already mentioned, the specified acceptance of the ring is for an edge emittance of 45,000 mm-mrad and half-width energy spread of 1.5%. To characterize the acceptance, it is necessary to track through the lattice including the effects of apertures; we have not so far performed these studies. However, we may estimate the acceptance using just the peak beta functions and dispersion. Since the maximum offset from the design axis, of a particle at the acceptance limit is well defined through (1), estimating the acceptance in this way should give reliable results. We have already seen that the dynamic aperture, neglecting the effects of errors, is outside the specified acceptance. We therefore need consider only the physical aperture.

The design work so far has assumed physical dimensions for the magnets and beam pipe as shown in Table 4. The limiting beam pipe radius is compared to the specified acceptance through one wiggler cell, estimated using equation (1), in Figure 11. Plots for other cells are very similar, except that the beam pipe radius is a constant 0.036 m.

Table 4: Parameters of the physical aperture

Dipole half-gap	0.040 m
Multipole pole-tip radius	0.040 m
Beam-pipe radius (outside wiggler)	0.036 m
Wiggler half-gap	0.020 m
Beam-pipe radius (through wiggler)	0.018 m

We see that the physical aperture is comfortably outside the specified acceptance, except for a short length near the center of the cell. It may be possible to correct this problem by retuning to reduce the vertical beta function in this region, or by opening the wiggler gap by a few millimeters.

For many of the magnets outside the achromat, a pole-tip radius of 0.04 m appears to be somewhat larger than necessary. However, the required gradients in the magnets are not large, and there may be little benefit in reducing the radius.

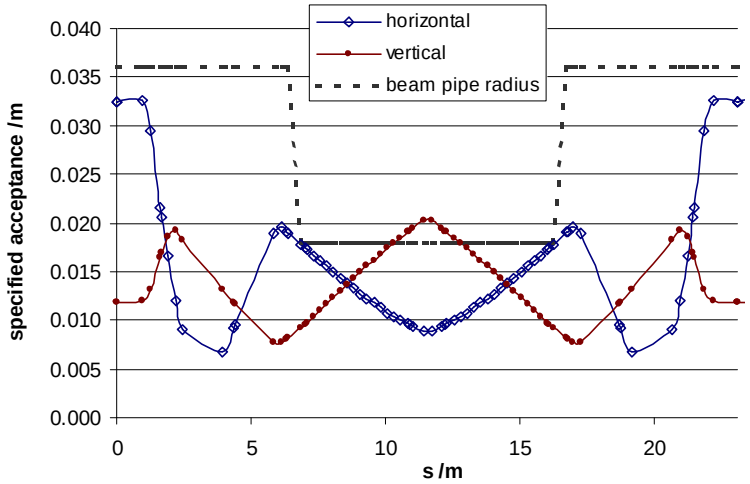

Figure 11

Horizontal and vertical specified acceptance through one wiggler cell. The solid curves show the horizontal and vertical edge beam size for edge emittance 45,000 mm-mrad, and momentum deviation 1.5%.

The acceptance is also an issue for the injection and extraction components. In the septa, the minimum separation between the beam centroids on either side of the current return blade is 77.8 mm. The horizontal beta function at this point is 14.47 m, so the edge beam size (from the center of the beam to its edge), assuming an edge emittance of 45,000 mm-mrad, is 18.3 mm. With a blade thickness[6] of 23 mm, this leaves a clearance of 9.1 mm between the edge of the injected beam and the blade. The tolerances on the extracted beam are much looser, because the beam is smaller by an order of magnitude.

In the quadrupole between the kicker and the septum, the kicked beam is offset by 37.1 mm. The beta function at this point is 3.347 m, so the edge beam size is 8.82 mm. With the present geometry, the beam pipe radius at this point would need to be increased to beyond 46 mm. We propose that the pole-tip radius of this quadrupole be specified at 50 mm to accommodate the increased size of the beam pipe.

4 Future Work

The pre-damping ring lattice design presented here meets the specifications for damping and dynamic acceptance. There are significant benefits in the double-bend achromat structure, over the racetrack lattice with TME arc cells that we have previously looked at. These include greater flexibility in design and (potentially) operation, reduced wiggler field and RF voltage, and control over the nonlinear dynamics through the use of harmonic sextupoles. Although the circumference of the lattice is slightly increased, and the design is less efficient when viewed simply in terms of numbers of magnets when compared to the racetrack TME, we feel that the structure presented here is to be preferred.

The acceptance of the present design appears to come close to that specified for the beam produced by the positron source. Some work needs to be done in the region of the

wiggler, which is currently limiting the acceptance to just below the specified values. Coupling effects are not expected to be a significant issue, since a fully coupled beam is acceptable.

Other areas that need to be addressed are as follows:

- optimization of the lattice in terms of length, location of linear components and working point in tune space;
- optimization of nonlinear dynamics;
- estimate of field quality tolerances in dipoles, quadrupoles and sextupoles;
- studies of the effects of orbit distortion on acceptance, and design of an orbit correction system;
- further design work on injection and extraction systems using specifications of components appropriate to the large acceptance;
- investigations of collective effects, including bunch lengthening and coupled bunch instabilities;
- detailed studies of the acceptance, using tracking with physical apertures.

5 Magnet Parameters

Name	Type	Location	Length	Pole-tip radius	Pole-tip field	Quadrupole gradient [c]	Sextupole Gradient [d]	Count
BB	Dipole		1.5	0.04	1.38326			20
BBCHP	Dipole	Chicane	0.6	0.04	0.98455			4
BBCHM	Dipole	Chicane	0.6	0.04	-0.98455			4
QAFW	Quadrupole	Wiggler cell achromat	0.3	0.04	0.55946327	2.117713		24
QADW	Quadrupole	Wiggler cell achromat	0.3	0.04	-0.5439103	-2.058841		24
QAFCH	Quadrupole	Chicane cell achromat	0.3	0.04	0.53059074	2.008423		2
QADCH	Quadrupole	Chicane cell achromat	0.3	0.04	-0.4825148	-1.826443		2
QAF	Quadrupole	Achromat	0.3	0.04	0.53015378	2.006769		6
QAD	Quadrupole	Achromat	0.3	0.04	-0.4804005	-1.81844		6
QM1W	Quadrupole	Wiggler cell straight	0.3	0.04	0.41893653	1.585783		12
QM4W	Quadrupole	Wiggler cell straight	0.3	0.04	-0.1703043	-0.6446459		6
QM0CH	Quadrupole	Chicane cell straight	0.3	0.04	-0.1347913	-0.51022		2
QM1CH	Quadrupole	Chicane cell straight	0.3	0.04	0.48636337	1.841011		2
QM4CH	Quadrupole	Chicane cell straight	0.3	0.04	-0.2159929	-0.8175889		1
QM0	Quadrupole	Straight	0.3	0.04	-0.14063	-0.5323208		6
QM1	Quadrupole	Straight	0.3	0.04	0.48371631	1.8309912		6
QM4	Quadrupole	Straight	0.3	0.05	-0.2815462	-0.85258		3
SX	Sextupole	Achromat	0.05	0.04	0.38996582		73.80606714	20
SY	Sextupole	Achromat	0.05	0.04	-0.2769972		-52.42529821	40
S1	Sextupole	Wiggler cell straight	0.05	0.04	-0.3125726		-59.158399	40
S2	Sextupole	Wiggler cell straight	0.05	0.04	0.16219005		30.696561	40

[c] Normalised: $\left(\partial B_y / \partial x\right) / B\rho$

[d] Normalised: $\left(\partial^2 B_y / \partial x^2\right) / B\rho$

6 Discussion of Phase Space Acceptance

6.1 Transverse Acceptance

The unnormalized emittance of a beam is given by the mean betatron action of particles in the beam:

$$\varepsilon_x = \langle J_x \rangle = \tfrac{1}{2}\left(\gamma_x \langle x^2 \rangle + 2\alpha_x \langle xx' \rangle + \beta_x \langle x'^2 \rangle\right)$$

Note that the single-particle emittance is defined as twice the betatron action:

$$\varepsilon_{sp,x} = 2J_x = \gamma_x x^2 + 2\alpha_x xx' + \beta_x x'^2$$

and that the maximum amplitude of betatron oscillations for this particle is then $\sqrt{\beta_x \varepsilon_{sp,x}}$. The beam coming from the positron source is not expected to be gaussian, and the distribution in the storage ring is not modified until the beam is damped close to equilibrium. For this reason, the ZDR gives the transverse acceptance in terms of an edge emittance, defined as the maximum betatron action of any particle in the beam[8]:

$$\varepsilon_{edge,x} = \max(J_x) = \tfrac{1}{2}\max(\varepsilon_{sp,x})$$

The maximum distance from the design orbit of a particle on the edge of the beam, and with a momentum deviation δ is therefore:

$$\hat{x} = \sqrt{2\beta_x \varepsilon_{edge,x}} + \eta_x \delta$$

This expression must be used to specify the required (physical and dynamic) aperture of the lattice[9].

For a non-gaussian distribution of particles within a beam, it is sometimes convenient to work with an effective rms emittance, defined through[10]:

$$\sigma_{eff} = 0.4\text{FWHM}$$

where FWHM specifies the full width of the distribution at half the maximum. Let us assume a flat distribution in *x*-*y* action space, up to some boundary $J_x^2 + J_y^2 = \varepsilon_{edge}^2$. The projection of the distribution onto either axis is parabolic, with FWHM $= \sqrt{3}\varepsilon_{edge}$. We then have (assuming no dispersion):

$$\varepsilon_{eff} = 0.4\sqrt{3}\varepsilon_{edge}$$

or

$$\varepsilon_{eff} \approx 0.7\varepsilon_{edge} \qquad (2)$$

The 0.09 m-rad acceptance[11] for the ZDR pre-damping ring design, refers to the normalized edge emittance of the injected beam[12]; the edge emittance gives the largest betatron action of any particle in the beam. We note that the charge per bunch is specified with a margin of 20% to allow for losses throughout the ring; however, there are no plans at present for how these losses may be safely absorbed[13].

The actual normalized edge emittance of the injected beam in the ZDR is[14] 0.06 m-rad. This is determined by the acceptance of the positron capture system, up to the entrance of the L-band 2 GeV booster linac[15]. The positron output from the target was calculated for the ZDR using the EGS program, and the phase-space distribution at the end of the capture linac was then found by ray-tracing[16]. Using (2), the value of 0.06 m-rad for the injected normalized edge emittance is consistent with Emma's assumption of 0.042 m-rad for the injected normalized rms emittance[3], and the value of 0.04 m-rad quoted by Sheppard et al[17].

Injection mismatches and other effects[18] (which may not be well understood) can increase the effective emittance by 50%; hence the acceptance value of 0.09 m-rad for the normalized edge acceptance. The specification for the injection errors is based on the assumption that the amplitude of the transverse beam "jitter" is equal to the edge beam size[19]. If the beam has edge emittance ε_{edge}, and we apply an action offset $\Delta J = \frac{1}{2}\varepsilon_{edge}$, (i.e. the action of every particle in the beam is increased by this amount) then the oscillation amplitude of the centroid of the beam is $\sqrt{2\beta\Delta J} = \sqrt{\beta\varepsilon_{edge}} = \sigma_{edge}$.

Studies of the pre-damping ring for the ZDR showed a dynamic aperture[20] significantly in excess of 0.09 m-rad, even in the presence of field and alignment errors, and a momentum aperture of 2%.

6.2 Longitudinal Acceptance

At the end of the positron capture linac (250 MeV), the energy spread is ±6%; this reduces to ±1.8% at the end of the booster linac[21]. An RF acceptance of ±1.8% would require an RF voltage in excess of 3.5 MV in the ZDR pre-damping ring design. Therefore, an energy compressor is included between the end of the L-band booster linac and the PPDR injector[22]. The energy compressor reduces the energy spread to ±1%, and also reduces the jitter to[23] ±0.2% rms. The RF voltage of the ZDR PPDR is then chosen to be 2.0 MV, which gives an acceptance of[24] ±1.5%. Another effect of the energy compressor system is that the bunch length, σ_z, increases from[25] 3.7 mm to 6.97 mm (note that the distribution in longitudinal phase space is highly non-gaussian).

Emma's design for the pre-damping ring[3] gives an equilibrium energy spread, σ_δ, of 0.089% and an equilibrium bunch length, σ_z, of 7.53 mm. Thus, the energy compressor improves the match to the energy bucket, though the energy spread is still a factor of ten too large.

6.3 Present Acceptance Values

The required acceptance values for the pre-damping ring most directly affect the designs of the magnets in the lattice, since these must have a sufficiently large bore to allow the passage of particles with betatron amplitudes and/or momentum deviations up to the acceptance values.

The values shown in Table 5 are the present specifications for the transverse and longitudinal acceptance of the positron pre-damping ring, and are significantly reduced from the ZDR values. The given values refer to the beam at the exit of the energy compressor, i.e. before the pre-damping ring injection systems. The transverse

acceptance gives the largest betatron action, including any transverse jitter in the action, for a particle at the exit of the energy compressor, that will be captured on injection into the damping ring. The energy acceptance gives the largest energy deviation for a particle at the exit of the energy compressor, that will be captured on injection into the storage ring. Note that the longitudinal phase-space of the injected and stored beams are highly mismatched, in the sense that a stored beam with an energy spread of 1% would have a bunch length of several centimeters, rather than several millimeters as is the case for the injected beam. The bunch length of the injected beam is therefore not an issue for the acceptance of the ring.

The transverse and longitudinal acceptances should be treated as directly additive, rather than adding in quadrature. In other words, the transverse acceptance should be independent of energy deviation: this gives the acceptance a "barrel" shape in phase space, rather than a "football" shape. The transverse dimension of the accepted beam is then given by:

$$\hat{x} = \sqrt{2\beta\varepsilon_{\max}} + \eta\delta_{\max}$$

where $\varepsilon_{\max}$ is the maximum accepted transverse emittance and $\delta_{\max}$ is the maximum accepted momentum deviation, both quantities including jitter. This formula determines the physical and dynamic aperture of the damping ring.

Table 5

Proposed acceptance values for next phase of pre-damping ring design work. These values refer to the positron beam at the exit of the energy compressor, in particular, before the pre-damping ring injection system.

Assumed injected transverse edge emittance (horizontal and vertical)	$\gamma\varepsilon_{edge}$	0.030 m-rad
Assumed injected transverse jitter (horizontal and vertical)	$\Delta\gamma J$	0.015 m-rad
Transverse acceptance (normalized edge emittance)	$\gamma\varepsilon_{\max}$	0.045 m-rad
Assumed injected energy spread (half width)		1%
Assumed injected energy jitter	$\Delta E/E$	±0.2%
Energy acceptance	$\delta_{\max}$	±1.5%
Assumed injected bunch length	σ_z	6.97 mm

References

[1] A. Wolski, "Lattice Description for NLC Main Damping Rings at 120 Hz", LCC-0061, April 2001.
[2] NLC Design Group, "Zeroth-Order Design Report for the Next Linear Collider" (ZDR), pp.143-148, SLAC Report 474, LBNL-PUB-5424, May 1996.
[3] P.Emma, "Preliminary e^+ Pre-Damping Ring Design for the NLC", SLAC Memorandum, March 24, 1999.
[4] R.A. Rimmer et al, "An RF Cavity for the NLC Damping Rings", Proceedings PAC 2001.
[5] S. de Santis, "Coupled Bunch Instabilities in the NLC Damping Rings", LCC-0069, April 2001.
[6] ZDR, page146.

[7] NLC Design Collaboration, "2001 Report on the Next Linear Collider: A Report Submitted to Snowmass '01", Chapter 5 "Injector Systems", June 2001.
[8] ZDR, page 164. I am grateful to Tor Raubenheimer for clarifying the definition of edge emittance for me.
[9] ZDR, page 145.
[10] ZDR, page 125.
[11] T. Kotseroglou et al, "Recent Developments in the Design of the NLC Positron Source", Proceedings PAC 1999.
[12] ZDR, pages 123-124.
[13] ZDR, page 120.
[14] ZDR, page 123.
[15] ZDR, pages 98-99.
[16] ZDR, pages 90-91.
[17] J.C.Sheppard et al, "The NLC Injector System", Proceedings, PAC 1999.
[18] ZDR, page 124.
[19] ZDR, pages 122-123.
[20] ZDR, page 164.
[21] ZDR, pages 98,100.
[22] ZDR, pages 132, 150-151.
[23] ZDR, page 123, Table 4-4.
[24] ZDR, page 132.
[25] ZDR, page 151, Table 4-9.